Crack propagation analysis in bituminous mixtures reinforced by different types of geogrids using digital image correlation

Reuber Arrais Freire, Hervé Di Benedetto, Cédric Sauzéat, Simon Pouget, Didier Lesueur

Crack propagation analysis in bituminous mixtures reinforced by different types of geogrids using digital image correlation

Reuber Arrais Freire [*a], Hervé Di Benedetto[a], Cédric Sauzéat[a], Simon Pouget[b], Didier Lesueur[c]

[a] *University of Lyon / ENTPE, Laboratory of Tribology and System Dynamics (LTDS) (UMR CNRS 5513), 3 Rue Maurice Audin, 69518 Vaulx-en-Velin, France;*

[b] *EIFFAGE Infrastructure, Direction R&D 8 rue du Dauphiné BP 357, 69960, Corbas Cedex, France,*

[c]*Afitexinov, 56 Route de Ferrossière, 38110 Saint-Didier-de-la-Tour, France / IMT Lille Douai, Institut Mines-Télécom, Univ. Lille, Centre for Materials and Processes, F-59000 Lille, France*

***Corresponding author:**

Reuber Arrais Freire

Laboratory of Tribology and System Dynamics (LTDS) (UMR CNRS 5513)

École Nationale des Travaux Publique de l'État (ENTPE) - University of Lyon

3 Rue Maurice Audin

69518 Vaulx-en-Velin,

France

Tel. : (+55) 8598175-9523

E-mail: reuber_freire@yahoo.com.br

Crack propagation analysis in bituminous mixtures reinforced by different types of geogrids using digital image correlation

In the rehabilitation of flexible pavements, the use of reinforcement by geogrids has substantially increased recently, aiming to extend the service life of pavements. This work evaluated the effect of fiberglass grid reinforcement on crack propagation of bituminous mixtures. To conduct the research, five different configurations of pre-notched beams constituted of two bituminous mixtures layers, with and without geogrid, were tested. Two different fiberglass geogrids, ultimate tensile strength (UTS) of 100 and 50kN/m, and emulsions as tack coat, made of bitumen pure and modify by polymer (SBS), were combined for the fabrication of three reinforced configurations. In addition, two unreinforced configurations were also fabricated. The first one was a single layer slab and the second one was bi-layered slab composed of two bituminous mixtures layers glued by a tack coat. The specimens were subjected to the four-point bending notched fracture (FPBNF) test, designed at the University of Lyon/ENTPE. A 3D Digital Image Correlation (DIC) technique was used to determine the strain field on specimen central length area during crack propagation. The results showed that the effect of geogrids was clearly noticeable when the specimen is subjected to high strain and the crack starts to propagate into the beams. DIC analysis allowed the observation of grid reinforcement effect on retarding the cracking propagation of bituminous mixtures layers.

Keywords: geogrid, reinforcement, bituminous mixtures, crack propagation

Subject classification codes:

1. Introduction

Interlayer reinforcement emerged in the 1930s as a solution to improve pavement structure performance [1]. Many interlayer systems have been analysed by the pavement community ever since, among the range of available commercialized products, such as sand

asphalt; SAMIs (Stress Absorbing Membrane Interlayers, composed by a blend of bitumen and rubber); fabrics or geotextiles; grids (steel, fiberglass and polymeric); and composites thereof [2, 3]. Recently, the use of geogrids has increased as a technical solution to rehabilitate pavements, extend their service life, and reduce maintenance costs [4]. Many works in the literature show that the reinforcement by geogrid can effectively retard the manifestation of cracking propagation in roadways [5-11]. Geogrid reinforcement was recommended since it could work as a strain-relieving component and effective to reflective cracking on the surface [5]. Reflective cracking is surface distress resulted from propagation of the cracks on an underneath damaged layer throughout the bituminous layer over it. In the cracking propagation analysis of bituminous mixtures, Fracture Mechanics concepts could be applied [12]. To evaluate the cracking resistance of reinforced bituminous mixtures in a prismatic beam shape in the laboratory different tests were proposed. Some authors used the three points bending test (3PBT) [8, 10, 13, 14]. Others used the four points bending test (4PBT) [8, 9, 15-18]. Other bending types of test could also be found in the literature [4, 7, 19-25].

In Italy, Pasquini et al. [7] conducted a work using geogrid-reinforced bituminous membranes as a method to prevent reflective cracking, for pavement rehabilitation. The specimens were composed of an old pavement layer and a new overlay with geocomposites within the interface. The tests called simulative reflective cracking (SRC) were performed in prismatic pre-notched specimens (3mm crack tip) produced in the laboratory. They were conducted at a temperature of 30°C and two amplitudes of loading (520 and 615N), with a rate of 21 cycles/min wheel rubber tire passing. From SRC tests, it was noticed that the geocomposites were effective in the anti-reflective cracking role since their performance was at least five times greater than the unreinforced specimen was. Canestrari et al. [8] performed 3PBT at monotonic displacement controlled loading and 4PBT at cyclic flexural tensile lading. The tests were carried out on double-layered bituminous mixtures specimens with geogrid reinforcement and at a temperature of 20°C. The authors used a fiberglass geogrid with and without polymer coating and a carbon fiber geogrid. Concerning the 4PBT, the authors observed an increase of approximately 3-fold (fiberglass) and 4-fold (carbon fiber) at 1kN load level,

compared to the unreinforced beam fatigue life (N_f). In addition, at a 1.5kN load level, 15-fold (fiberglass) and 6-fold (carbon fiber) was observed. Concerning 3PBT, the authors noticed that the fiberglass geogrid was more effective in retarding crack propagation from the bottom to the top of the specimen.

In France, located at the IFSTTAR APT facility, there is an outdoor circular carousel dedicated to full-scale pavement experiments. Thus, some work concerning geosynthetics reinforcement has been conducted in this facility. Hornych et al. [26] constructed four pavement sections, three reinforced by fiberglass geogrid and one without reinforcement. Standard dual wheels applied the load of 65 kN and the loading speed was 6 rounds/minute (43 km/h). The temperatures varied between 20 and 28°C. In crack monitoring results, the reinforced section with the film as tack coat was the first to present cracks, followed by the unreinforced section. The reinforced section with the bitumen tack coat did not present cracks. Nguyen et al. [27] referring to the full-scale characterization using IFSTTAR APT facility concluded that the fiberglass geogrid, placed near the bottom of the bituminous mixture layer significantly improves the fatigue life. However, the bond quality between the geogrid and the bituminous mixture layers is essential to occur the reinforcement. Lastly, Arsenie et al. [17, 28] studied the improvement in the fatigue resistance of bituminous mixtures by the utilization of coated fiberglass geogrid as reinforcement. The authors used the Four Point Bending Tests (4PBT) with beam containing two interface-geogrid, tested at a temperature of 10°C and frequency of 25Hz. In the first work, an increment in the fatigue life between 33.5% and 45.5% was observed and in the second work, the increase in the fatigue life (N_f) was 60%, based on fatigue Wohler curves.

Digital Image Correlation (DIC) technique was found to be a useful tool allowing the identification of different failure mechanisms during the crack propagation stage in reinforced beams and showing the strain-relieving capacity of geogrids [8, 13]. Recently, the DIC analysis has been successfully employed for the cracking propagation analysis of bending beam tests [9, 11, 18, 29-31]. This technique is more precise and gives more cracking information comparing to the classical analysis using strain gauges. Using DIC, the

information of a whole surface could be obtained, whereas, strain gauges are only able to measure data in local points.

Saride & Kumar [18] used DIC to analyse the 4PBT carried out in double-layer specimens reinforced with polyester grid (PET) and a glass-grid composite (GGC), and an unreinforced specimen. The specimens were composed by an extruded old asphalt as bottom layer and new asphalt overlay as top layers. Two pre-notch sizes were evaluated (25 and 40mm) along with specimens without it. Cyclic loading with 550kPa of magnitude at 25°C (room temperature) was used to obtain specimen fatigue properties. From DIC analysis, a tensile strain reduction was observed in the reinforced specimens of about 35-70% at the crack tip. Moreover, the fatigue life of the reinforced specimens was highly increased. Kumar & Saride [11] conducted a work aiming at evaluating the cracking resistance potential of double-layer reinforced beams. The test was carried out using the direct tensile strength test (DTT), at 20, 30, and 40°C with a constant vertical displacement rate of 1mm/min, and analysed using DIC. The results indicated an increase in the crack resistance potential due to the reinforcement, especially at 20°C. DIC analysis presented a reduction of tensile strain at the crack tip for reinforced specimens. The specimen with glass-grid reinforcement tested at 20°C presented a 2.7 times reduction when compared to the single-layer specimen tested at the same temperature.

The literature evidenced an improvement in fatigue and crack propagation resistance due to the geogrid reinforcement, especially fiberglass geogrids. However, the characterization found were mostly at high temperatures (around 20°C), which difficult the interpretation of the cracking propagation phenomenon due to bituminous viscous behaviour. Hence, this work aimed at evaluating the effect of fiberglass geogrid reinforcement, presence, type, and tack coat, in crack propagation of bituminous mixtures layers. Moreover, the effect of geogrid ultimate tensile strength (UTS) and the SBS modification of the emulsion tack coat was evaluated. To this end, four-point bending notched fracture (FPBNF) tests designed at the University of Lyon/ENTPE [32] were carried out. To better analyse the tests, 3D Digital Image Correlation (DIC) technique was used to calculate the strain field on specimen central length area, during the crack propagation as well as its tip location.

2. Materials and Experimental Protocol

2.1 Materials

The French bituminous mixture BBSG 0/10 (*Béton Bitumineux Semi-Grenu*) was used to conduct the experimental campaign. This mixture was classified according to the European standards [33] and is normally used for surface courses. The BBSG 0/10 gradation curve is presented in Figure 1(a). It is composed of rhyodacite and rhyolitic mineral aggregates, limestone filler, and 20% of reclaimed asphalt pavement (RAP) containing 4.75% of aged bituminous binder. These aggregates were mixed with 4.40% of a new bituminous binder classified as 35/50 by its penetration. The total bituminous binder content (aged + new) in the mixture was 5.53% per total weight of the mixture.

The geogrids used to reinforce the bituminous mixtures were Notex Glass®, presented in Figure 1(b). It was composed of fiberglass yarns knitted to a light polyester veil, with a bituminous coating on both sides. The grids had a square mesh opening of 25mm in the two directions. Two types of geogrids were used in this work with UTS of 50kN/m (C 50/50) and 100kN/m (C 100/100), in two perpendicular directions. These UTS were obtained at the failure point of 3% of strain in grids tensile characterization tests carried out for fabrication quality control. Lastly, a bituminous emulsion 160/220 by penetration [34] was used as a tack coat to glue the geogrid in the middle part of the slabs. A slab configuration was fabricated with bituminous emulsion modified by a styrene-butadiene-styrene (SBS) block copolymer.

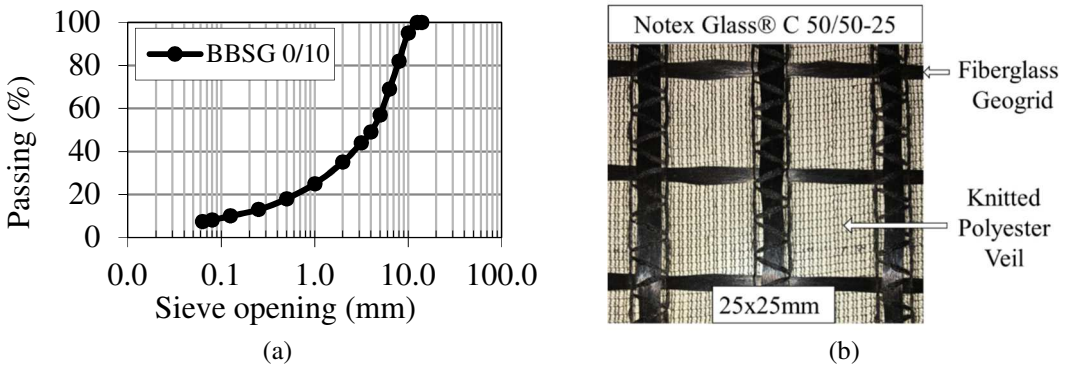

Figure 1. Components of tested specimen: (a) bituminous mixture gradation curve; (b) fiberglass geogrid Notex Glass® C 50/50-25

2.2 Specimens preparation

Five different slab configurations, with dimensions 600 of length, 400 of width, and 150mm of depth, were compacted using a French wheel compactor [35]. Configuration A did not have an interface, while B, C, D, and E had interface and were denoted by bi-layered slabs. Configuration B had only the tack coat of emulsion made of pure bitumen at a residual rate of 290g/m². Whereas configurations C, D, and E were made with geogrid (50 and 100kN/m of UTS) and the tack coat (emulsion bitumen pure and with SBS) at a residual rate of 800g/m², and were denoted by reinforced slabs.

The fabrication of configuration A slab followed the classical procedure described in the standard [35], since it was composed of a single layer slab, without interface/reinforcement. Concerning the reinforced slabs, they were fabricated by first compacting half-height slab (75mm) at a temperature of 180°C (for mixing and compaction) and cooling down for 24h. Then, the first tack coat application was done (400g/m²), followed by the geogrid placement. Afterward, the second tack coat application was done (400g/m²) on the geogrid surface. Finally, a period of 24h was waited so that the breaking process occurs in the emulsion before the second half-height (75mm) slab compaction. Figure 2 presents the steps of slab fabrication procedure.

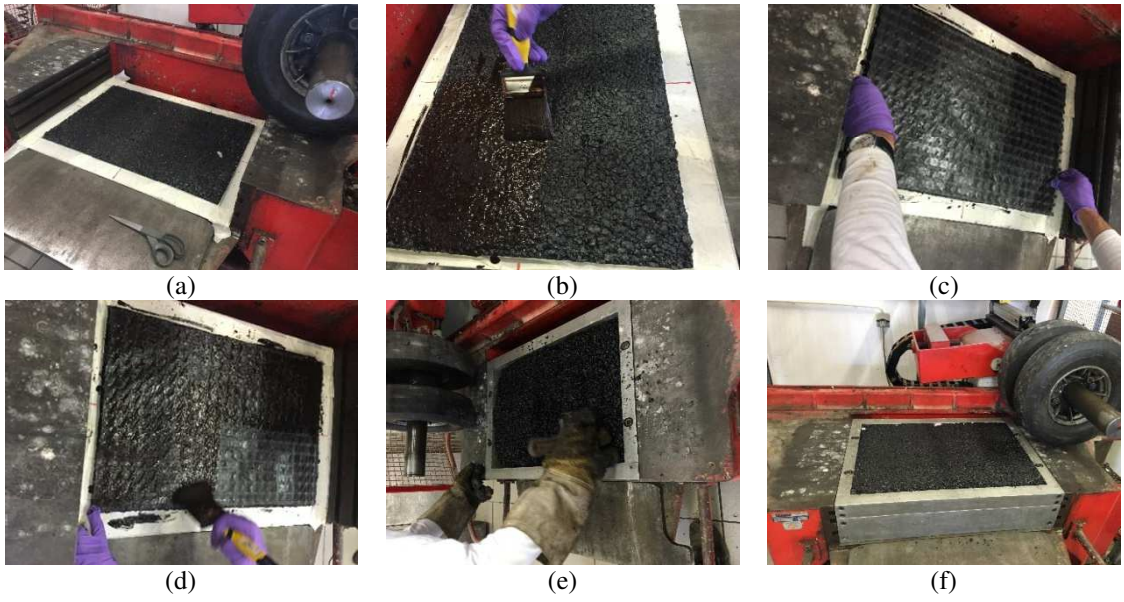

(a) (b) (c)

(d) (e) (f)

Figure 2. Slab fabrication of reinforced bi-layered bituminous mixture: (a) First layer compaction; (b) Emulsion first application; (c) Fiberglass geogrid placement, (d) Emulsion second application, (e) Upper layer fabrication, and (f) Final compaction.

From each slab, three prismatic bars, with dimensions 550 of length, 70 of width, and 110mm of depth were sawn. Moreover, a 20mm long, 1mm thick notch was made in its centre-bottom. Finally, to improve DIC accuracy, a speckle pattern was applied on the rectangular area located in the central length of the beam, with a thin layer of white acrylic paint and a spray of black paint on it. Figure 3 illustrates the slab composition and the final reinforced beam used for the tests. Detailed information on the specimen composition, as well as air voids content calculated in the bituminous mixture and are presented in Table 1. The air voids in reinforced specimens were obtained by removing the grid and the tack coat weights and volumes from the specimen specific gravity calculation.

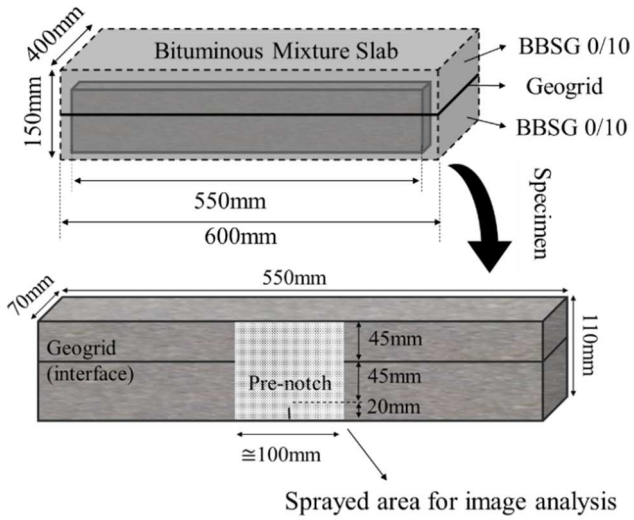

Figure 3. Detail of beam specimen position from the slab, obtained from sawing and prepared for testing

Table 1. Tested specimens composition and air voids in bituminous mixtures

Configuration	Specimen	Interface		Air Voids (in bituminous mixture layers) (%)
		Composition	Tack coat rate (residual binder)	
A	A1	Not applicable	Not applicable	6.3
	A2			7.8
B	B1	Pure bitumen	292g/m²	5.4
	B2			6.5

C	C1	Pure bitumen and GG 100kN/m		6.2
	C2			4.1
	C3			4.7
D	D1	Pure bitumen and GG 50kN/m	2×400g/m²	6.1
	D2			4.3
E	E1	SBS-modified bitumen and GG 100kN/m		3.7
	E2			3.9

2.3 Four-point bending notched fracture (FPBNF) test

The test was performed in a servo-hydraulic press. The press produces axial loading from its actuator. The actuator displacement was measured by an integrated transducer and used for controlling the loading applied during the tests. The press was equipped with a load cell with 50kN maximum capacity. Moreover, three Linear Variable Differential Transducers (LVDT) were placed on the top of the beam, two of them directly above the lower supports (LVDT1 and LVDT3) and another one in the beam centre length (LVDT2) to measure the vertical displacement in these three points. Beam's deflection was not only obtained with the LVDT2 measurement but also using the LVDT1 and LVDT3 measurements, which allowed estimating the punching effect of the lower supports into the beam. Thus, beam deflection was calculated according to Equation (1).

$$Deflection = LVDT2 - \frac{LVDT1 + LVDT3}{2} \quad (1)$$

Figure 4 presents a scheme containing the devices used to perform the test. Four-point bending notched fracture (FPBNF) tests designed at the University of Lyon/ENTPE were carried out. More test details can be found in previous works [27, 32, 36]. A thermal chamber was coupled to the press [37, 38] allowing temperature control. The specimen surface temperature was measured using one thermal gauge (PT100 temperature probe) fixed on the specimen surface. Furthermore, during the presented experimental campaign, two added cameras (CCD Pike F-421B/C) targeting the sprayed area were positioned outside the thermal chamber. These two cameras allowed performing the 3-dimension DIC analysis.

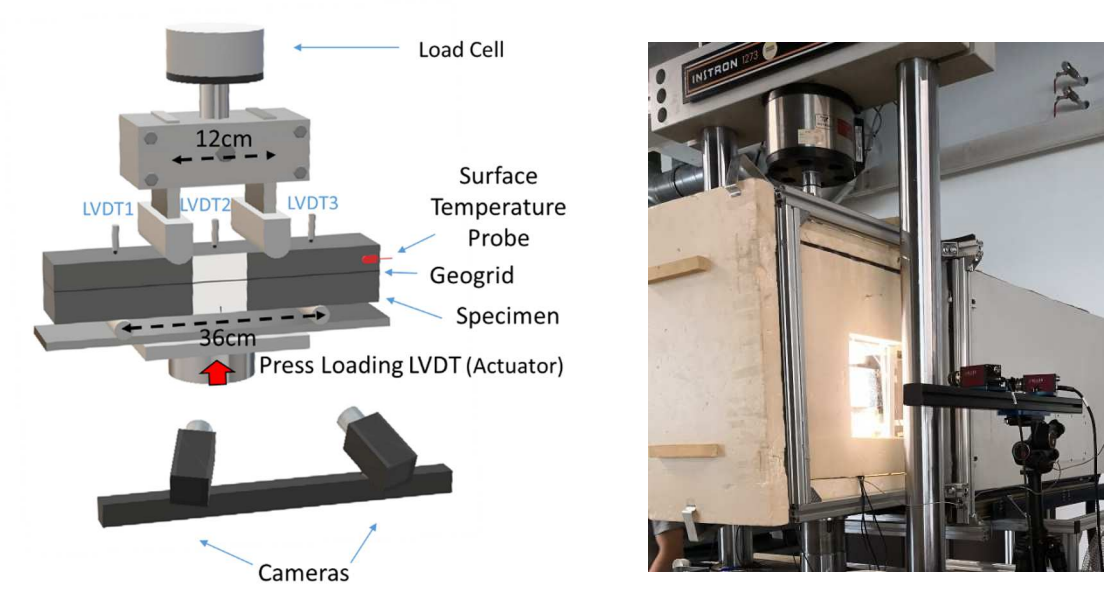

(a) (b)

Figure 4. Experimental test device and procedure for FPBNF test: (a) scheme and measurement device location; (b) Thermal chamber and cameras set up

The specimens were conditioned at -5°C overnight in a freezer and transferred to the press, where one additional hour of temperature conditioning at -5°C was done. The FPBNF test was performed at a constant rate of actuator displacement of 0.2mm/min. The test was divided into two steps. First, two "small" cycles of loading/unloading were performed at the same displacement rate with a small force amplitude (1kN peak and 0,3kN valley) to ensure the good setting of contact between specimen and supports. Second, a constant rate of actuator displacement loading was performed until the complete crack propagation throughout the specimen height. Figure 5(a) presents a plot containing the actuator displacement input and the force (P) response measured during the test for sample A2. An energy approach was also used to evaluate crack propagation resistance of different specimens' configurations. In this approach, the area below the curve force versus actuator displacement corresponds to the necessary mechanical energy to propagate the crack throughout the specimen's height. Figure 5(b) illustrates the area used for this calculation and presents the energy restitution rate (G_f) equation, where W_0 is the area below the curve, w is the beam width (m), H is the beam height (m) (dimensions of beam's section), and a_0 is the pre-notch size (m).

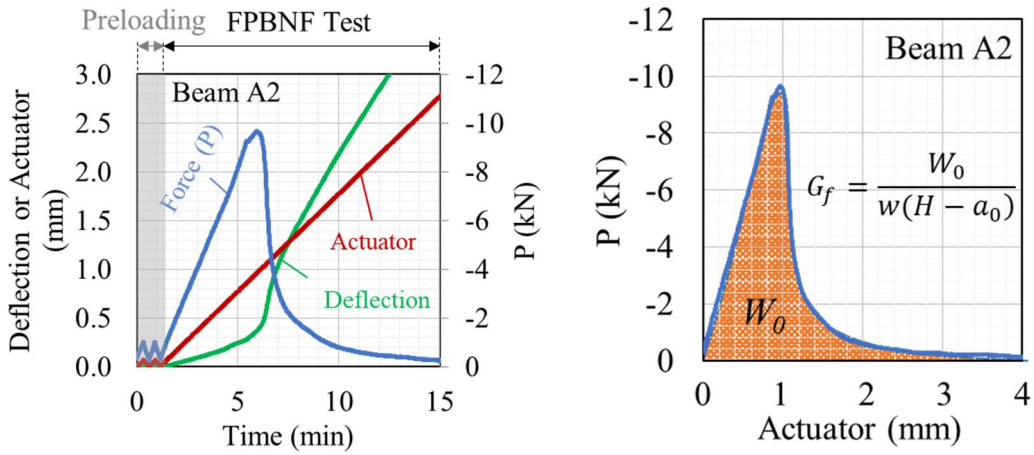

Figure 5. Test on sample A2: (a) actuator displacement, force, and deflection versus time; (b) force versus actuator displacement and the area below the curve (W_0) used to calculate the energy restitution rate (G_f)

3. Digital image correlation (DIC) analysis

DIC is an optical and contactless measurement technique used to compute the displacement on a specific area of analysis [39]. From simultaneous monochromatic digital images acquired with the aid of two cameras, a 3D displacement field was obtained by image correlation. Each picture is an arrangement of pixels in different shades of grey. The displacement was calculated by comparing subsets of virtual squares containing a small amount of pixel in original and deformed states at different instants of time [39-41]. The strain field is also deduced by the derivation of displacement. The software VIC 3D 7 Correlated Solutions, Inc. was employed to perform the image correlation treatment. For each test, one couple of pictures (one from each camera) was taken every 3s during the tests. A subset size of 21 pixels and a filter size of 15 pixels were used for DIC analysis in VIC 3D.

Using the software, horizontal lines were created every 2mm of specimen height starting from the notch tip. The initial height of the crack tip was the notch size (a_0). Each virtual gauge line was composed of 100 virtual points, and for each point, the horizontal strain (ε_{xx}) was calculated. A positive sign means an extension of the analysed point of the specimen (tensile strain) while a negative sign stands for a contraction.

The cracking appearance criterion, useful for crack tip identification, was the same used and validated considering back analysis in previous work at the University of Lyon/ENTPE

[37, 38]. It is given by the maximum boundary value, ε_{xx} = 0.01m/m. As soon as this value was measured in one (or more) point of the gauge line, the crack was considered passing this line (propagating higher in the beam). This allows following the crack tip during the test. Furthermore, for each virtual gauge line, the average strain ($\varepsilon_{xx\,AVG}$) of its points was calculated and plotted as a function of the specimens' height. As the crack propagates through the central region of the specimen, a reduction of points was applied and only the points presented within the central 60mm were considered in the calculation of ($\varepsilon_{xx\,AVG}$) and analysis. Figure 6 presents an explanation of the adopted analysis methodology and results at one instant during the test on specimen C, having a geogrid of 100kN tensile strength.

However, when the crack was open and its tip had already passed the analysed line, the strain measured from DIC could be imprecise leading to errors in the analysis. Thus, a correction in the $\varepsilon_{xx\,AVG}$ of the line in this situation was performed: all the points in the line located at ±5mm around the crack were removed from $\varepsilon_{xx\,AVG}$ calculation. In order to locate this range of points, the maximum strain measured ($\varepsilon_{xx\,MAX}$) is found for a given instant of time t, and the coordinate x of the point containing $\varepsilon_{xx\,MAX}$ is used. Thus, if $\varepsilon_{xx\,MAX} \geq$ 0.01m/m (crack criterion), the removed points are those between the range of x±5mm around the point of $\varepsilon_{xx\,MAX}$. Figure 6 illustrates the mentioned procedure.

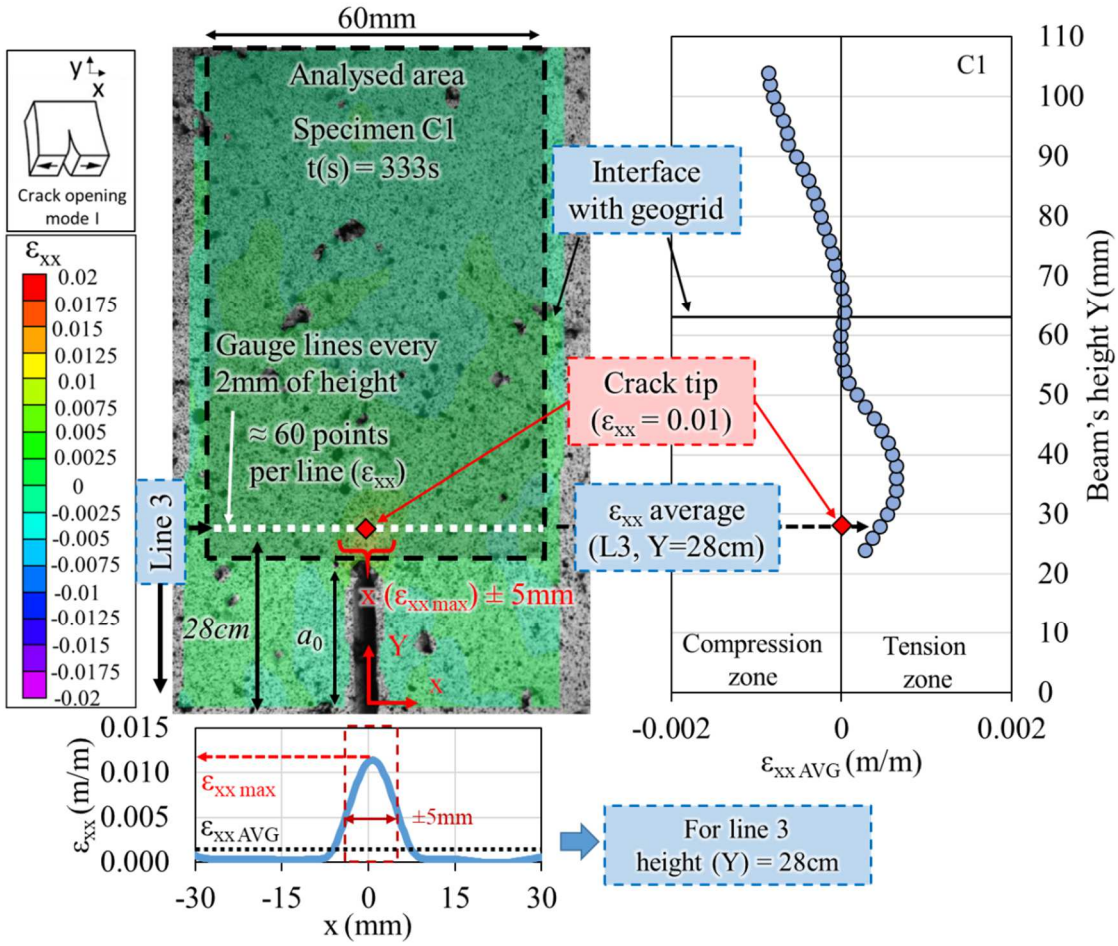

Figure 6. Explanation of procedure of analysis performed with Digital Image Correlation (DIC) technique (specimen C1, t=333s)

4. Crack Propagation Test Results

4.1 Force versus deflection curves

The Force versus Deflection curve (calculated using Equation 1) was plotted for the five tested specimens in Figure 7. Curve peak indicates approximately the crack initiation and from this point, the crack starts to propagate. Similar curves in this region confirmed that the presence of the geogrid did not noticeably influence the load peak value. This same result was observed in Canestrari [8].

It is possible to notice a difference between the reinforced specimens and the unreinforced ones in the post-peak part of the curve. The fiberglass geogrid improves the crack propagation resistance of bituminous mixtures. Concerning configuration A (no interface) and B (interface with bitumen pure), similar curves were observed, which indicates very similar

behaviour. Two different values of force in the plateau regime were observed in the reinforced specimens: one for the geogrid with UTS of 50kN (D specimens) and another for the geogrid UTS of 100kN (C and E specimens). The force plateau observed for C and E specimens was approximately twice when compared to the one observed for specimens D, which was consistent with the ratio between the UTS of them. In addition, the curves also indicated that from 1.5mm of beam's deflection, most of the effort was taken by the geogrids. This result indicated that the UTS of the geogrid directly influences the load capacity of the beam.

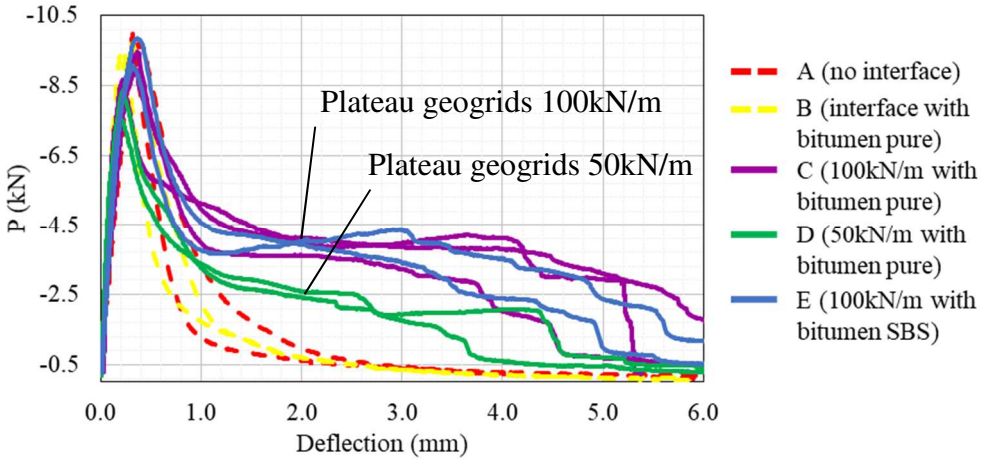

Figure 7. Force versus deflection curve results for tested specimens (cf. Table 1)

From the results of tests on specimens A and B without geogrid, presented in Figure 7, it is clear that for deflection higher than about 2mm the bituminous layer(s) did not support any load because the crack was propagated over the whole thickness. It is then possible to give an evaluation of the geogrid effect during the tests C, D, and E, by assuming that only the geogrid supports loading from this point (2mm of deflection). A calculation was done to verify this hypothesis. The equilibrium of moments in the central section is written in Equation 2 considering that compressive force is supported by the upper bituminous mixture layer at a given point located at a distance h of the geogrid (hinge in Figure 8). In the plateau regime, just before total failure, the geogrid reaches its load strength (F_{GGfail}). The ductile failure of the geogrid can be mobilised as large strain values exist in this material. The maximum force supported by the geogrid during the bending F_{GGfail} was calculated by considering that the grids were subjected to their UTS, 50 and 100kN/m. Moreover, each specimen contained

approximately 3 yarns of the grid resisting the bending, and there were 40 yarns/m since their mesh openings were 25mm. Thus, F_{GGfail} was 3.75kN for 50kN/m geogrid (configuration D) and 7.5kN for 100kN/m geogrid (configurations C and E). Equation 3 gives the expression of h in the plateau regime, h_P. The obtained values are given in Table 2 for specimens C, D, and E. These values are higher than 3cm and lower than 4cm, which is quite physically realistic and could be considered as a validation of the simplified postulated hypothesis. This result indicates that the force plateau of reinforced specimens was due to the geogrid mobilization at large deflection during the test.

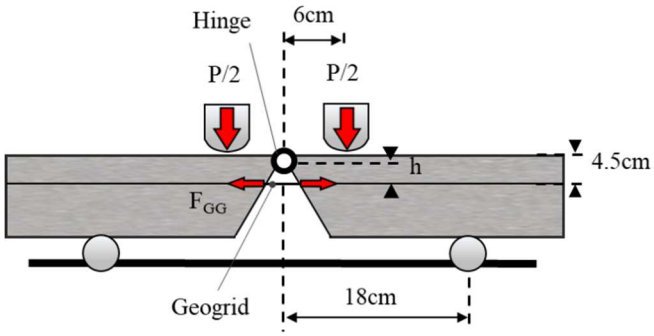

Figure 8. Illustration of four points bending beam pivoting around a hinge, supported only by the geogrid.

$$F_{GGfail} \cdot h_P - 6 \cdot (P_P) = 0 \quad (2)$$

It comes on the plateau regime:

$$h_P = \frac{6 \cdot (P_P)}{F_{GGfail}} \quad (3)$$

Where P_P is the value of force obtained for the plateau regime taken at 0.2cm of deflection, and h_P is the hinge height in the plateau regime expressed in centimetres.

Table 2. Forces measured on the plateau regime (taken at 2mm of deflection) and corresponding plateau pivot height (h_P)

Specimen	P_P (kN)	h_P (cm)
C1	3.7	3.0
C2	4.1	3.3
C3	4.0	3.2
D1	2.4	3.9
D2	2.5	4.0

E1	4.0	3.2
E2	3.9	3.1

4.2 Energy restitution rate

Figure 9 presents the energy restitution rate (G_f) obtained for all tested specimens. This result represents the mechanical energy to propagate the crack throughout the specimen's height. Thus, it was expected higher G_f in the tests of specimens reinforced by geogrid. The results obtained concerning unreinforced specimens (configurations A and B) presented much lower G_f than the reinforced specimens (configurations C, D, and E). Configuration C (100kN/m and pure bitumen tack coat) needed approximately 2.6 times more energy to propagate the crack in relation to A (no interface) and 3.3 times more in relation to B (interface with pure bitumen tack coat). Concerning configuration D (50kN/m and pure bitumen tack coat), approximately 1.5 times more in relation to A and 1.9 times more in relation to B were obtained. Lastly, in configuration E (100kN/m and bitumen-SBS tack coat) the relations obtained were 2.5 times more to A and 3.2 times more to B. These results indicated that more fracture energy is required for reinforced specimens due to geogrid presence. This parameter could be associated with the reflective cracking resistance of reinforced bituminous mixtures layers. Thus, the results suggested that geogrid reinforcement was effective to combat reflective cracking in bituminous mixtures layers. Moreover, the unreinforced bi-layer specimen (configuration B) performed 22% lower when compared to the single-layered specimens (configuration A). This performance decrease suggested that the interface presence weakened the specimen performance against reflective cracking, and showed up the importance of high-quality interface adhesion. Comparing the reinforced specimens, configurations C and E needed a similar amount of energy to propagate the crack and approximately 1.7 times more than D. This result indicated that the UTS of the geogrid influenced the performance of the specimens much more than the type of tack coat used. UTS could be translated to stiffness since both geogrids failed at the same strain level (3%) in their tensile characterization. Therefore, higher stiffness resulted in better performance to reduce reflective cracking in bituminous mixtures layers, similar

conclusion as obtained by Kumar and Saride [11].

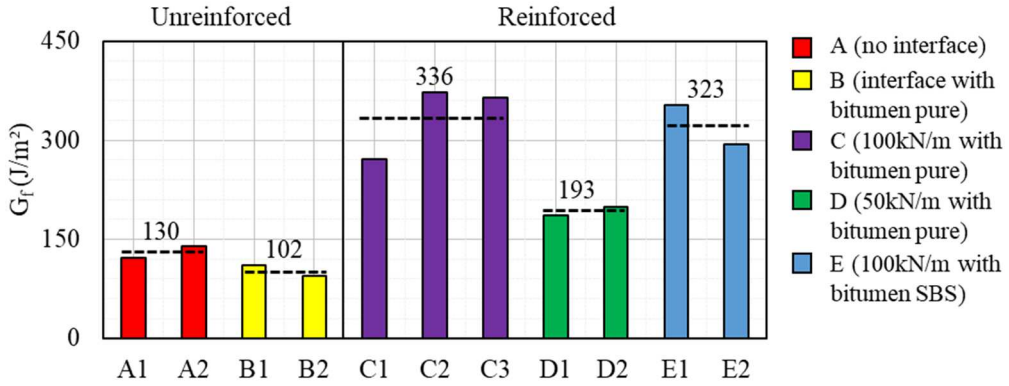

Figure 9. Energy restitution rate (G_f) obtained for the tested specimens

4.3 DIC analysis

DIC measurement was verified considering a strict calibration process using LVDT. This step is not detailed as it is a compulsory step included in all good experimental campaigns. An example of comparison between LVDT and DIC measurements concerning specimen A2 is given in the appendix. Figure 10 presents images of all tested specimens at the end of their respective tests, achieved when the force measured decreased to -0.5kN, to observe the crack shape. Concerning unreinforced specimens (configurations A and B), it can be observed that the cracks presented a rather straight vertical path from the bottom to the top. The same observation can be made concerning the specimens of configuration E and specimen C1. However, concerning the other two specimens of configuration C and the specimens of configuration D, the crack had his path deviated at the interface by the geogrid.

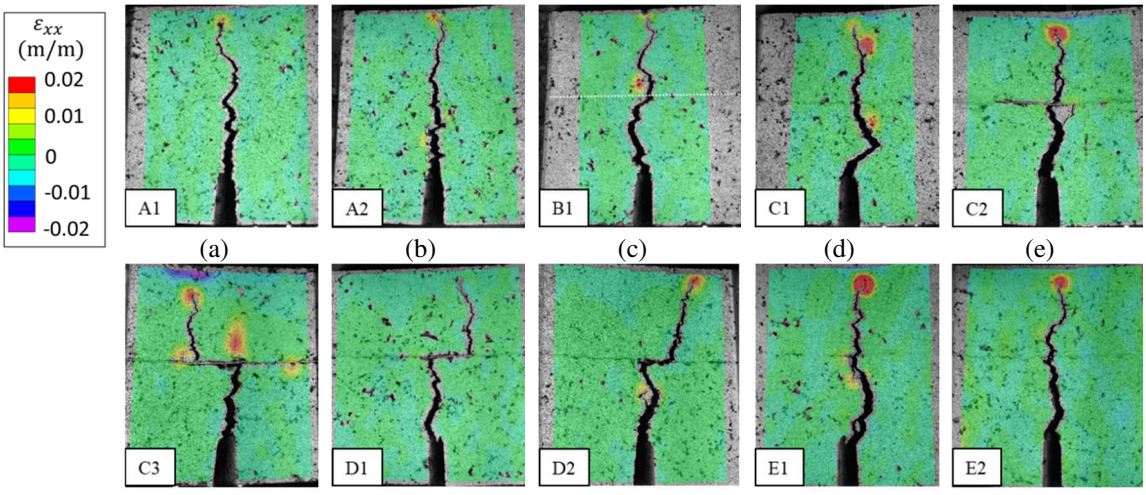

Figure 10. Treated images of tested specimens at the end of crack propagation

Figure 11(a) presents the evolution of the crack tip height (a) as a function of the beam deflection for unreinforced specimens A (no interface) and B (interface with pure bitumen tack coat). For these specimens, overlapped curves with no discontinuity were obtained. Similar to the results of force versus deflection, the presence of a tack-coat-only interface did not affect the evolution of crack tip height and configuration B yields identical curves as configuration A, despite the difference obtained with the energy approach discussed in the previous section.

Figure 11(b) presents the results for unreinforced specimens but includes also the results obtained in the tests conducted with specimens of configuration C (100kN/m and pure bitumen tack coat). The curve for C1 was similar to the curves for unreinforced specimens. However, concerning specimens C2 and C3, a clear cracking retard was observed since the beams presented more deflection before crack propagation from the interface to the upper layer. At the interface level, the deflection measured for the unreinforced specimens was approximately 0.7mm, whereas C2 and C3 measured approximately 1.1mm, which means 1.6 times higher, comparing them. This is indicative of crack retarding due to the presence of geogrid.

Figure 11(c) presents the graphic of unreinforced specimens but including the results obtained in the tests conducted with specimens of configuration D (50kN/m and pure bitumen tack coat). Again, distinct curve shapes were observed. For both D1 and D2, a discontinuity was observed when the crack reached the interface level. From this point, a cracking delay was noticeable. The deflection measured in the tests of D specimens was approximately 1.05mm when the crack reached the interface level, which was 1.5 times higher than specimens A and B at the same point of analysis.

Lastly, Figure 11(d) presents the plot for unreinforced specimens but including the results obtained in the tests conducted with specimens of configuration E (100kN/m and SBS-modified tack coat). In this case, the curves presented a similar shape to specimens A and B, even if the configuration E specimens show slightly higher deflection than the unreinforced

specimens do. The deflection measured for configuration E results were approximately 0.85mm when the crack reached the interface level, which is 1.2 times higher than specimens A and B at the same point of analysis.

It should be noted in Figure 11 a good repeatability of the tests for each configuration since the tests resulted in overlapped curves of specimens with the same configuration (except specimen C1). To conclude, each time the crack path had only a little deviation from the vertical direction of propagation (seen in Figure 10), the same crack height versus deflection curve was observed (tests A, B, C1, and E). Thus, the result presented in Figure 11 was directly related to the ability of interface-geogrid to deviate the crack path during its vertical propagation (results of beams C2, C3, and D). As a result, the crack height versus deflection curve shows a discontinuity at the interface, meaning that the propagation of the crack in the upper layer was delayed. However, this ability depends on the characteristics of the used tack coat and was not observed for the SBS modified tack coat (configuration E).

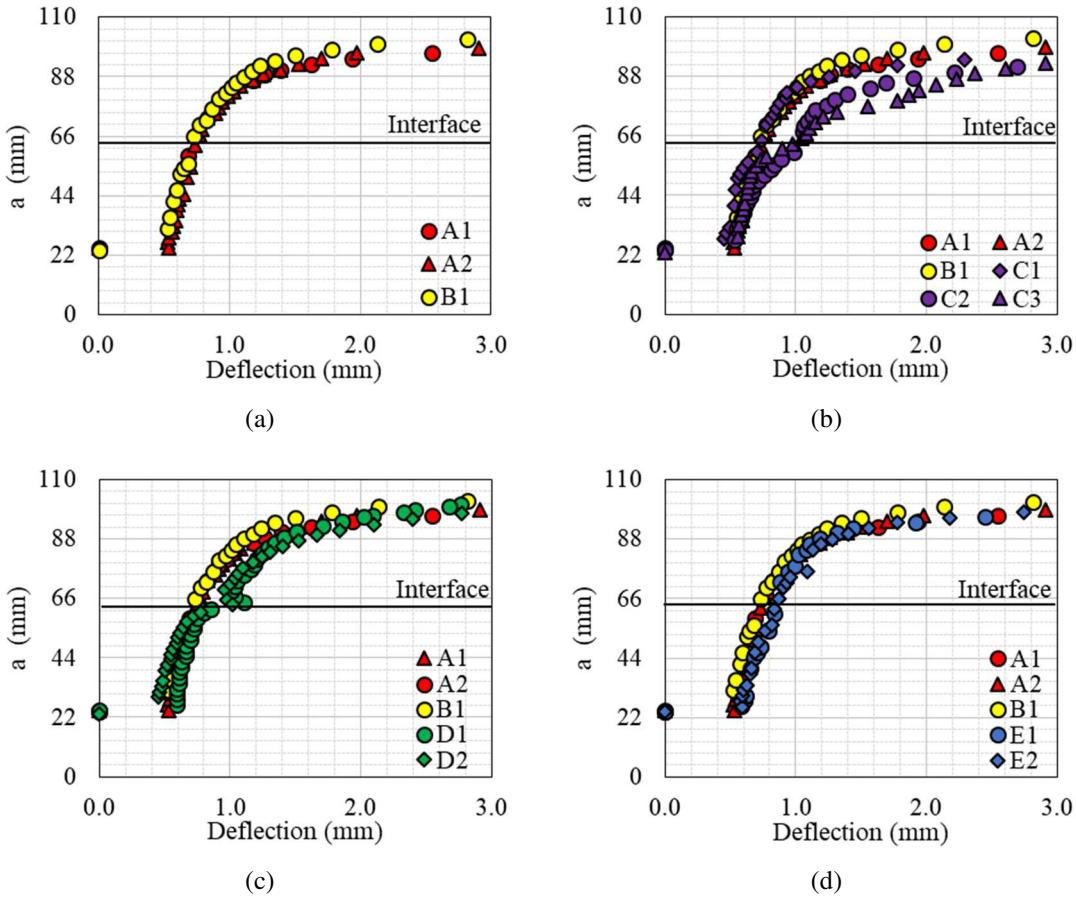

Figure 11. Crack tip height "a" versus beam deflection: (a) unreinforced configurations containing interface (B) and no interface (A), (b) configuration C (geogrid of 100kN/m) together with unreinforced configurations, (c) configuration D (geogrid of 50kN/m) together with unreinforced configurations, and (d) configuration E (geogrid of 100kN/m with SBS-modified tack coat) together with unreinforced configurations

Figure 12(a) presents the *P* versus deflection curve obtained for unreinforced specimen B1 (interface with pure bitumen tack coat). In this figure, three specific locations were chosen: (1) peak of the curve, deflection = 0.3mm, t = 306s, (2) Post peak at a deflection = 0.56mm, t = 333s and (3) Post peak at a deflection = 1mm, t = 360s. The first point represents the moment when the crack was about to start to propagate, the second one was the moment where the crack tip reached the interface, and the last one represented a moment when the crack was almost at the end of the propagation.

Figure 12(b) presents the DIC analysis at point 1. The DIC treated image (left) and the plot of maximum horizontal strain ($\varepsilon_{xx\ MAX}$) (right) show a strain concentration at the tip of the pre-notch. Figure 12(c) presents the analysis at point 2. At this stage, the crack propagated and the tip reached approximately a height of 66mm. At this point, in both graphics, average strain ($\varepsilon_{xx\ AVG}$) (middle), and maximum strain ($\varepsilon_{xx\ MAX}$) (right), a gap was observed between the curves below and above the interface. This gap indicates a slight slip at the interface between the bituminous mixture layers when the crack tip was reached. Figure 12(d) presents the analysis at point 3. In this case, the crack propagated in the upper layer, and its tip reached approximately 88mm of height. In this last point, the gap disappeared from the average strain graphic. However, in the maximum strain graphic, the gap was bigger.

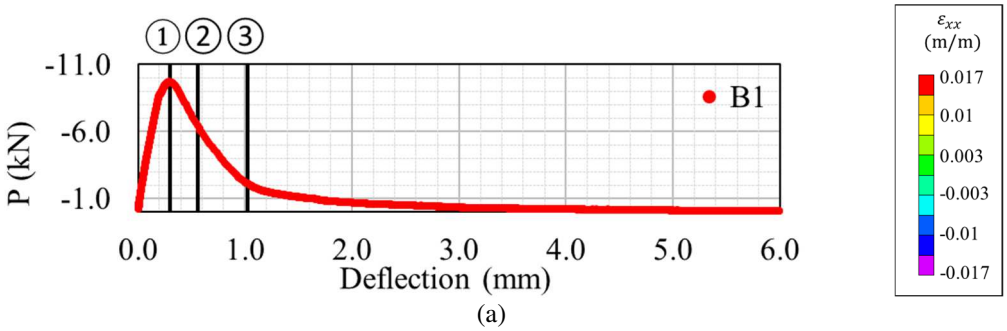

(a)

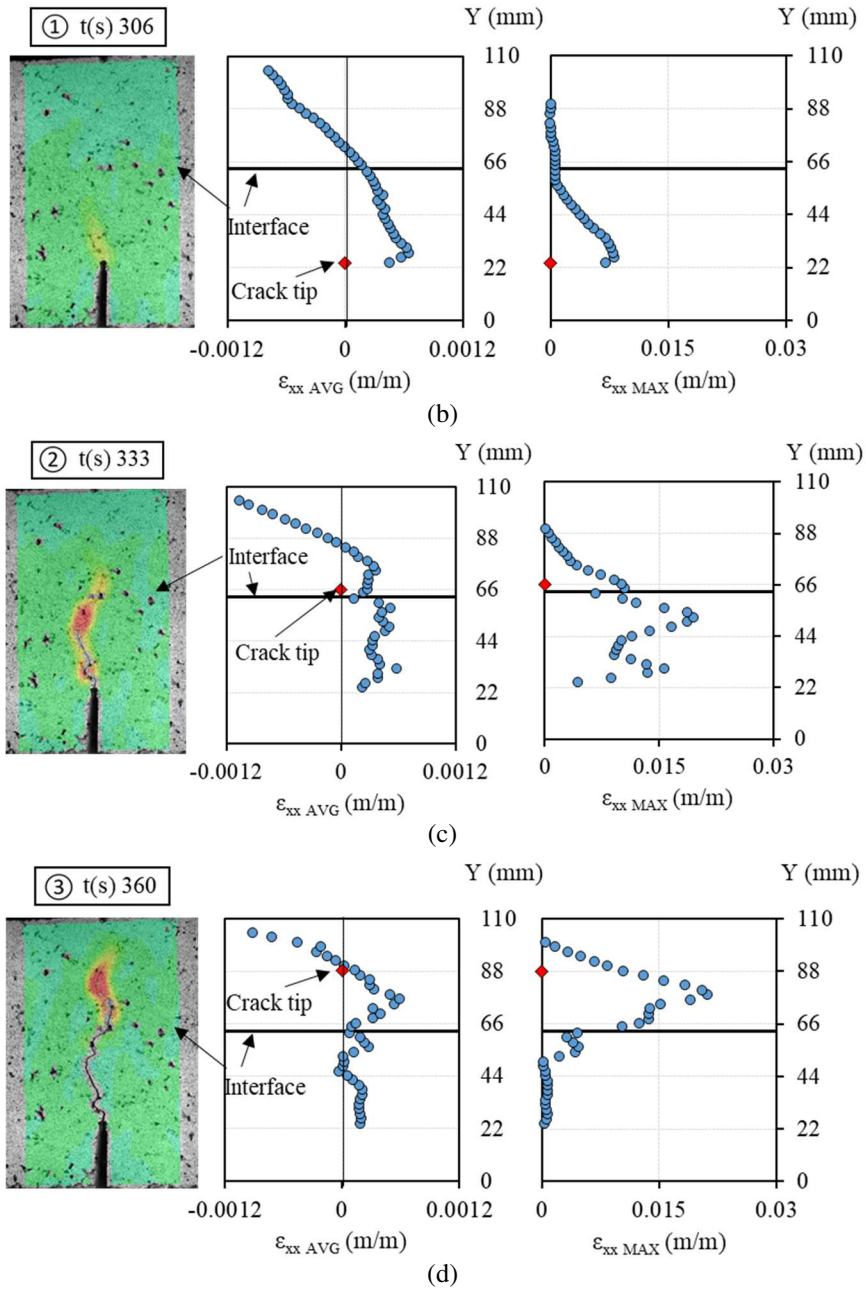

Figure 12. Results for test on unreinforced specimen B1 (interface with pure bitumen tack coat): a) Global load versus deflection curve; b, c, d) Crack and horizontal strain field obtained with DIC analysis (left); average strain values ($\varepsilon_{xx\ AVG}$) (middle) and maximum strain values ($\varepsilon_{xx\ Max}$) (right) versus beam height for positions 1 (b), 2 (c) and 3(d) indicated in (a).

Regarding a reinforced specimen, the previous analysis was performed on sample D2 (50kN/m and pure bitumen). Figure 13(a) presents the obtained curve *P* versus deflection. In this figure, the four points chosen for the analysis of average and maximum strains throughout the beam height are indicated: (1) peak point, deflection = 0.25mm, t = 306s, (2) post-peak point at a deflection = 0.45mm, t = 348s, (3) post-peak point at a deflection = 1mm, t = 456s, and (4)

post peak-point at a deflection = 2.6mm, t = 804s. The first point represents the moment when the crack was about to start the propagation, the second one was the moment when the geogrid started being mobilized, the third one was the beginning of force plateau period, and the last one was the end of the force plateau period.

Figure 13(b) presents the DIC analysis at point 1. The average strain at the interface level at this moment of the test was zero because the interface with geogrid was placed very close to the neutral axis of the beam. This result shows that the geogrid was not mobilized until the beginning of crack propagation. Moreover, it explained why the results obtained for all the specimens, regardless of their constitution were the same until the peak of force.

Figure 13(c) presents the analysis at point 2. In this case, the crack propagated and its tip reached approximately 29mm of height. Concerning the average strain graphic, the upper layer behaved as a beam subjected to bending alone (triangular stress distribution). However, a high strain level at the interface indicates that the geogrid was mobilized at this point. From the maximum strain graphic, it is noticeable that the strain was more concentrated in the lower layer than in the upper layer. Moreover, there is no gap caused by the interface suggesting that there was no slip in the interface.

Figure 13(d) presents the analysis at point 3. At this point, the crack propagated and its tip reached approximately 77mm of height. When the crack tip reached the interface, it was deviated from its original path due to the geogrid presence. At this moment, it was noticeable that even when the crack tip passed through the geogrid, the strain value (extension) is very high at the interface level, it was approximately 0.001m/m on average with a maximum of 0.017m/m. This result was another evidence that the geogrid was highly mobilized during the force plateau and, therefore, being responsible for it.

Finally, Figure 13(e) presents the analysis at point 4. At this point, the crack propagated and its tip reached approximately 97mm of height. At this moment, the geogrid was the one responsible for supporting the load since no more strain could be measured on the bituminous mixture except in the free of the crack upper part of the specimen where high compressive strain exists indicating compression stress. This visual DIC analysis validates the simplified

hypotheses made previously (Equation 3). Table 2 the hinge is located at 3.9 cm from the geogrid, which corresponds to the value obtained in Figure 13(e). The decrease of load P after point 4 was related to the geogrid deterioration. At the end of the test, it was observed that the geogrid was broken.

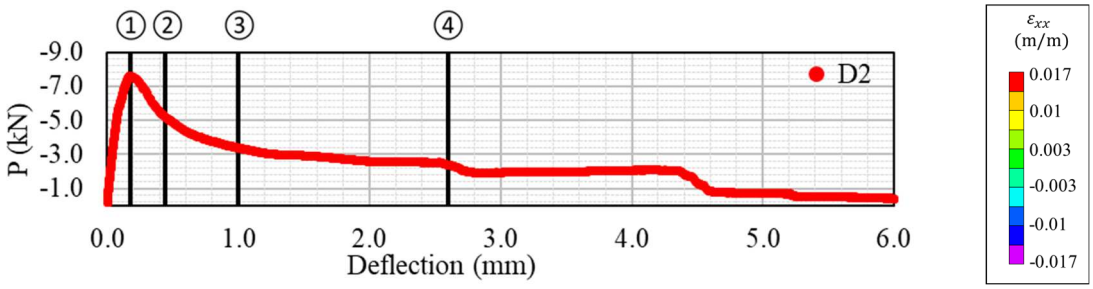

(a)

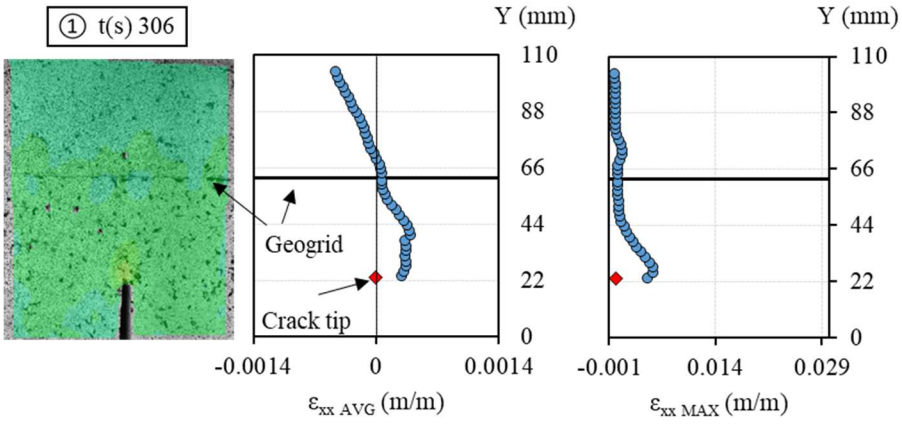

(b)

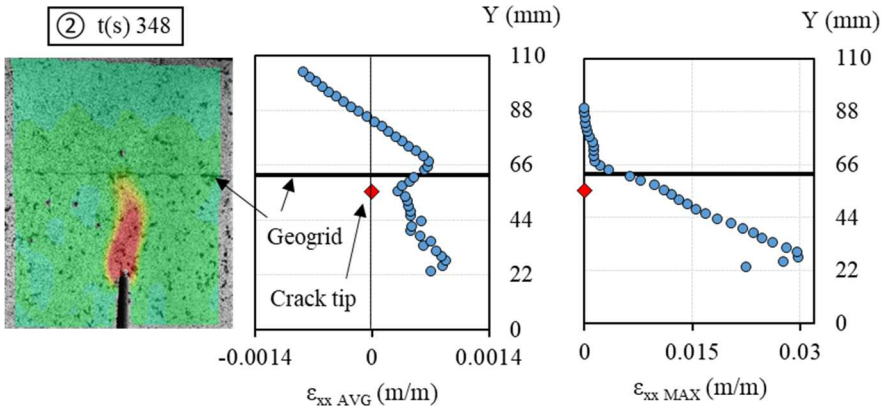

(c)

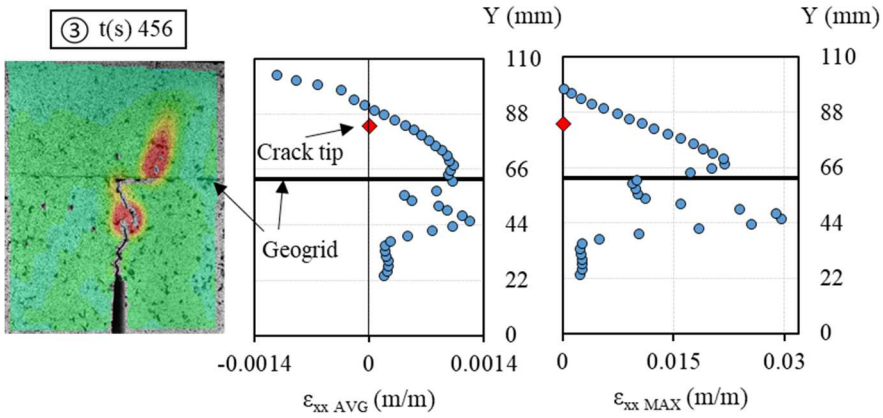

(d)

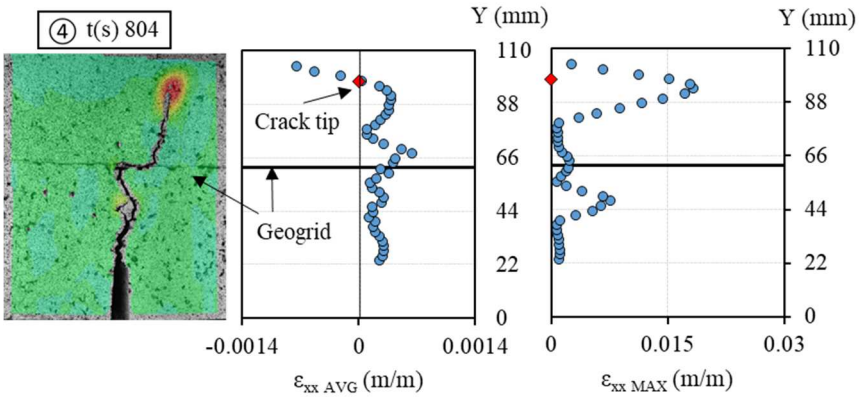

(e)

Figure 13. Results for test on specimen D2 (interface with 50 kN/m geogrid): a) Global load versus deflection curve; b, c, d, e) Crack and horizontal strain field obtained with DIC analysis (left); average strain values ($\varepsilon_{xx\,AVG}$) (middle) and maximum strain values ($\varepsilon_{xx\,MAX}$) (right) versus beam height for positions 1 (b), 2 (c), 3(d) and 4(e) indicated in (a).

5. Conclusions and Recommendations

This work presented an evaluation of the effect of fiberglass geogrid reinforcement to reduce de reflective cracking of bituminous mixtures layers. Moreover, geogrid ultimate tensile strength (UTS) and the SBS modification of the emulsion bitumen (tack coat) were also evaluated. The major conclusions are listed below:

- The presence of an interface, containing or not a geogrid, does not influence the peak load, which is an indication of crack propagation initiation.
- Geogrids increase the resistance of the beam to crack propagation. A plateau zone is observed where the load is mainly controlled by geogrid strength (crack-bridging). The increase in geogrid UTS increased the plateau value for the geogrids adopted in the study.

- Digital Image Correlation (DIC) analysis was useful and efficient for calculating the strain field and the crack tip position during the test. It allowed explaining what physically happens on the beam surface around crack location thanks to a powerful visual tool.
- Even after the crack has crossed the interface, the geogrid was still highly capable of supporting the load. The crack could propagate for more than 2 cm over the interface before the geogrid breaks.
- The non-linearity observed in $\varepsilon_{xx\ AVG}$ as a function of crack height during the test was caused by geogrid influence, interface thickness, and tack coat quantity and quality.
- Modelling and quantification of the plateau phenomenon observed with the geogrid interface were proposed. The simple postulated hypotheses were validated by the DIC analysis.

Following these conclusions, some recommendations and perspectives for future research are presented hereafter:

- Cyclic loading test at a temperature of 10°C and a frequency of 10Hz should be performed to assess the fatigue cracking behaviour of reinforced specimens
- Construction and monitoring of a field trial reinforced by the fiberglass geogrids and emulsions tack coat used in this study, to validate the results obtained.

References

[1] Beckham, W.K. and W.H. Mills (1935). "Cotton-Fabric-Reinforced Roads." Engineering News Record, Vol. 115, No. 13, pp. 453-455.

[2] Vanelstraete, A., and Franken, L. (1997). "Prevention-of-reflective-cracking-in-pavements" (RILEM TC 157 PRC report).

[3] Cost Action 348, (2006) "Reinforcement of pavements with steel meshes and Geosynthetics (REIPAS)". COST Action 348 Final report.

[4] De Bondt A.H., (2012) "20 years of research on asphalt reinforcement. Achivements and future needs." Proceeding of the 7th International RILEM Conference on Cracking in Pavements, Delft.

[5] De Bondt, A. H., (1999) "Anti-reflective cracking design of reinforced asphaltic overlays", PhD thesis, Delft University of Technology, Netherland.

[6] Khodaii, A., Fallah S., Fereidoon Moghadas Nejad, F.M. (2009). "Effects of geosynthetics on reduction of reflection cracking in asphalt overlays". Geotextiles and Geomembranes 27, pp.1–8. DOI:10.1016/j.geotexmem.2008.05.007

[7] Pasquini, E., Pasetto, M., & Canestrari, F. (2015).” Geocomposite against reflective cracking in asphalt pavements: laboratory simulation of a field application.” Road Materials and Pavement Design, 16:4, 815-835, DOI:10.1080/14680629.2015.1044558.

[8] Canestrari, F., Belogi, L., Ferrotti, G. and Graziani, A. (2015) “Shear and flexural characterization of grid-reinforced asphalt pavements and relation with field distress evolution.” Materials and Structures, 48(4), 2015, 959–975, DOI: 10.1617/s11527-013-0207-1

[9] Safavizadeh, S.A., Wargo, A., Guddati, M., & Kim, Y.R., (2015) "Investigation of reflective cracking mechanisms in grid-reinforced asphalt specimens using four-point bending notched beam fatigue tests and digital image correlation." Transp. Res. Record, (2507), 29-38. DOI: 10.3141/2507-04

[10] Zofka A., Maliszewski, M. and Maliszewska, D. (2016) "Glass and carbon geogrid reinforcement of asphalt mixtures." Road Materials and Pavement Design, vol, pp. DOI:10.1080/14680629.2016.1266775

[11] Kumar V.V. & Saride S., (2018) “Evaluation of cracking resistance potential of geosynthetic reinforced asphalt overlays using direct tensile strength test.” Construction and Building Materials, V. 162, P. 37-47, ISSN 0950-0618, DOI:10.1016/j.conbuildmat.2017.11.158.

[12] Gauthier, G. & D. A. Anderson. 2006. “Fracture mechanics and asphalt binders.” Road Materials and Pavement Design (EATA 2006): 9-36.

[13] Romeo, E. Freddi, F. and Montepara, A. (2014) “Mechanical behaviour of surface layer fibreglass-reinforced flexible pavements”, International Journal of Pavement Engineering, 15:2, 95-109, DOI: 10.1080/10298436.2013.828838

[14] Graziani A., Sangiorgi C., Canestrari F. (2016) “Fracture Characterization of Grid-Reinforced Asphalt Pavements.” 8th RILEM International Conference on Mechanisms of Cracking and Debonding in Pavements. RILEM Bookseries, vol 13, 66-67, DOI: 10.1007/978-94-024-0867-6_9

[15] Virgili A., Canestrari F., Grilli A., Santagata F.A., (2009) “Repeated load test on bituminous systems reinforced by geosynthetics”, Geotextiles and Geomembranes, Volume 27, Issue 3, 187-195, DOI: 10.1016/j.geotexmem.2008.11.004.

[16] Ferrotti G, Canestrari F, Virgili A, Grilli A (2011). “A strategic laboratory approach for the performance investigation of geogrids in flexible pavements”. Construction and Building Materials, 25(5):2343–2348. DOI: https://doi.org/10.1016/j.conbuildmat.2010.11.032.

[17] Arsenie, I.M., Chazallon, C., Duchez, J.L. and Hornych, P. (2017) “Laboratory characterisation of the fatigue behaviour of a glass fibre grid-reinforced asphalt concrete using 4PB tests.” Road Materials and Pavement Design, 18:1, 168-180, DOI:10.1080/14680629.2016.1163280

[18] Saride S. & Kumar V.V., (2019) “Reflection Crack Assessment Using Digital Image Analysis” In: Latha G. M. (eds) Frontiers in Geotechnical Engineering. Developments in Geotechnical Engineering. Chapter 8. Springer, Singapore. DOI: 10.1007/978-981-13-5871-5_8

[19] Komatsu, T., Kikuta, H., Yoshinobu, T., and Muramatsu, E. (1998). “Durability assessment of geogrid-reinforced asphalt concrete.” Geotextiles and Geomembranes, Vol. 16, 257-271.

[20] Millien, A., Dragomir, M. L., Wendling, L., Petit, C., & Iliescu, M. (2012). “Geogrid interlayer performance in pavements: Tensile-bending test for crack propagation.” In T. Scarpas, N. Kringos, I. L. Al-Qadi, & A. Loizos (Eds.), 7th RILEM International Conference on Cracking in Pavements (Vol. 2, pp. 1209–1218). Dordrecht: Springer.

[21] Obando-Ante, J. & Palmeira, E.M., (2015) “A Laboratory Study on the Performance of Geosynthetic Reinforced Asphalt Overlays.” International Journal of Geosynthetics and Ground Engeneering, 1: 5, DOI: 10.1007/s40891-014-0007-x

[22] Fallah S., Ali Khodaii, A. (2015). “Reinforcing overlay to reduce reflection cracking; an experimental investigation”. Geotex. and Geomemb., 43, pp.216-227. DOI: 10.1016/j.geotexmem.2015.03.002

[23] Gonzalez-Torre I., Calzada-Perez M. A., Vega-Zamanillo A., Castro-Fresno D., (2015) “Evaluation of reflective cracking in pavements using a new procedure that combine loads with different frequencies.”, Const. and Build. Mat., Vol. 75, 368-374, DOI:10.1016/j.conbuildmat.2014.11.030.

[24] Norambuena-Contreras J., Gonzalez-Torre I., (2015) “Influence of geosynthetic type on retarding cracking in asphalt pavements.” Construction and Building Materials, Vol 78, Pages 421-429, ISSN 0950-0618, https://doi.org/10.1016/j.conbuildmat.2014.12.034.

[25] Nejad F. M., Asadi S., Fallah S., Vadood M., (2016) “Statistical-experimental study of geosynthetics performance on reflection cracking phenomenon”, Geotextiles and Geomembranes, Volume 44, Issue 2, 178-187, DOI:10.1016/j.geotexmem.2015.09.002.

[26] Hornych, P., Kerzrého, J. P., Sohm, J., Chabot, A., Trichet, S., Joutang, J. L., & Bastard, N. (2012). "Full scale tests on grid reinforced flexible pavements on the French fatigue carrousel." Proceedings of the 7th international RILEM conference on cracking in pavements, Delft.

[27] Nguyen M. L., Sauzéat C., Di Benedetto H., Tapsoba N., (2013) "Validation of the Time-Temperature superposition principle for crack propagation in bituminous mixtures", Materials & Structures, volume 46, Issue 7, pp. 1075-87, DOI: 10.1617/s11527-012-9954-7.

[28] Arsenie, I.M., Chazallon, C., Themeli, A., Duchez, J.L., and Doligez, D. (2012) "Measuraments and predictions of fatigue behavior of glass fiber reinforced bituminous mixtures". Seventh International RILEM Conference on Cracking in Pavements. Volume 2 pp.653-664. DOI: 10.1007/978-94-007-4566-7

[29] Kumar V V, Saride S. (2017) "Use of Digital Image Correlation for the Evaluation of Flexural Fatigue Behavior of Asphalt Beams with Geosynthetic Interlayers". Transportation Research Record. 2631(1):55-64. DOI: 10.3141/2631-06

[30] Saride S. & Kumar V.V., (2017) "Influence of geosynthetic-interlayers on the performance of asphalt overlays on pre-cracked pavements, Geotextiles and Geomembranes" Volume 45, Issue 3, 2017, Pages 184-196, ISSN 0266-1144, DOI: 10.1016/j.geotexmem.2017.01.010.

[31] Saride S. & Kumar V.V., (2019) "Estimation of Service Life of Geosynthetic-Reinforced Asphalt Overlays from Beam and Large-Scale Fatigue Tests," Journal of Testing and Evaluation 47, no. 4: 2693–2716. DOI: 10.1520/JTE20170605

[32] Nguyen, M. L. & Sauzéat, C. & Di Benedetto, H. & Wendling, L. (2008) "Investigation of cracking in bituminous mixtures with a 4 points bending test". Proceedings of the 6th Rilem Int. Conf. On cracking in Pavement, Ed. Al-Qadi, Scarpas, Loizos, Balkema Pub., pp. 284-293, Chicago. DOI:10.1201/9780203882191.ch28.

[33] NF EN 13108-1 (2016) "Mélanges bitumineux. Spécifications pour le matériau." Association Française de Normalisation (AFNOR), Paris. (In French)

[34] NF EN 12591 (2009) "Bitumen and bituminous binders." Specifications for paving grade bitumens. Association Française de Normalisation (AFNOR), Paris. (In French)

[35] NF EN 12697-33 (2019) "Bituminous mixtures - Test method - Part 33: Specimen prepared by roller compactor." Association Française de Normalisation (AFNOR), Paris. (In French)

[36] Nguyen M. L., Di Benedetto H., Sauzéat C., (2016) "Crack propagation characterization of bituminous mixtures using four-point bending notched specimen test", Road Materials and Pavement Design, Vol 17-1, pp. 70-86, DOI: 10.1080/14680629.2015.1063535.

[37] Pedraza, A., (2018) "Propriétés thermomécaniques d'enrobés multi-recyclés" (in French), PhD thesis, University of Lyon/ENTPE, France.

[38] Pedraza, A., Di Benedetto, H., Sauzéat, C., Pouget, S., (2019) "Fracture properties of multirecycled asphalt mixes from four-point bending test using digital image correlation and back calculation", Journal of Testing and Evaluation, 47 (5), pp. 3275-3288.

[39] Sutton, M. A., W. J. Wolters, W. H. Peters, W. F. Ranson, and S. R. McNeill. (1983) "Determination of Displacements Using an Improved Digital Correlation Method." Image and Vision Computing, 1 (3): 133-139.

[40] Attia, T., Di Benedetto, H., Sauzeat, C., Olard, F. and Pouget, S. "Hollow cylinder apparatus to characterize interfaces between pavement layers." 71st RILEM Annual Week & ICACMS, Chennai, India, Vol. 4, 2017, pp. 401-410.

[41] Attia T., Di Benedetto H., Sauzéat C., Pouget S., (2020) "2T3C HCA, a new hollow cylinder device using Digital Image Correlation to measure properties of interfaces between asphalt layers" Construction and Building Materials, Vol. 247, 118499, DOI:10.1016/j.conbuildmat.2020.118499

List of notations and abbreviations

a	crack tip height, mm
a_0	pre-notch size, mm
BBSG	*béton bitumineux semi-grenu* (semi-coarse hot asphalt mixture)
DIC	digital image correlation
F_{GGfail}	maximum force supported by the geogrid during the bending, kN
FPBNF	four-point bending notched fracture
G_f	energy restitution rate, J/m²
GG	geogrid
H	beam height, m
h	distance between the hinge and interface, cm
h_P	distance between the hinge and interface in the plateau regime, cm
LVDT	linear variable differential transducers
P	force, kN
P_P	value of force obtained for the plateau regime, kN
RAP	reclaimed asphalt pavement
SBS	styrene-butadiene-styrene
UTS	ultimate tensile strength
w	beam width, m
W_0	area below the curve P vs Actuator
Greek symbols	
ε_{xx}	horizontal strain
$\varepsilon_{xx\ AVG}$	average strain for a virtual gauge line
$\varepsilon_{xx\ MAX}$	maximum strain measured on a virtual gauge line

Appendix

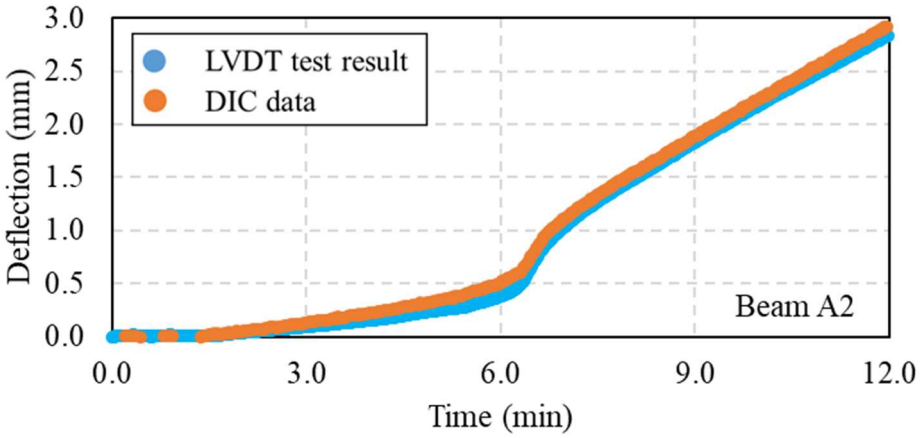

Figure 1. Comparison of measured (LVDT) and predicted (DIC) deflection for unreinforced beam A2